HHS Public Access

Author manuscript

Nat Methods. Author manuscript; available in PMC 2019 May 09.

Published in final edited form as:

Nat Methods. 2018 September ; 15(9): 700–706. doi:10.1038/s41592-018-0081-4.

Induction of Myelinating Oligodendrocytes in Human Cortical Spheroids

Mayur Madhavan[1,*], **Zachary S. Nevin**[1,*], **H. Elizabeth Shick**[1], **Eric Garrison**[2], **Cheryl Clarkson-Paredes**[3], **Molly Karl**[2], **Benjamin L.L. Clayton**[1], **Daniel C. Factor**[1], **Kevin C. Allan**[1], **Lilianne Barbar**[1], **Tanya Jain**[4], **Panagiotis Douvaras**[4], **Valentina Fossati**[4], **Robert H. Miller**[2], and **Paul J. Tesar**[1]

[1]Department of Genetics and Genome Sciences, Case Western Reserve University School of Medicine, Cleveland, Ohio 44106, USA

[2]Department of Anatomy and Regenerative Biology, George Washington University School of Medicine and Health Sciences, Washington, DC 20037, USA

[3]Nanofabrication and Imaging Center, George Washington University School of Medicine and Health Sciences, Washington, DC 20037, USA

[4]The New York Stem Cell Foundation Research Institute, New York, New York 10019, USA

Abstract

Organoid technologies provide an accessible system to examine cellular composition, interactions, and organization in the developing human brain, but previously have lacked oligodendrocytes, the myelinating glia of the central nervous system. Here we reproducibly generate oligodendrocytes and myelin in human pluripotent stem cell-derived “oligocortical spheroids”. Transcriptional, immunohistochemical, and electron microscopy analyses demonstrate molecular features consistent with maturing oligodendrocytes by 20 weeks in culture, including expression of MYRF, PLP1, and MBP proteins and initial myelin wrapping of axons, with maturation to longitudinal wrapping and compact myelin by 30 weeks. Promyelinating drugs enhance the rate and extent of oligodendrocyte generation and myelination, while oligocortical spheroids generated from patients with a genetic myelin disorder recapitulate human disease phenotypes. Oligocortical spheroids

Correspondence and requests for materials should be addressed to P.J.T. (paul.tesar@case.edu).

*These authors contributed equally to this work

Author Contributions

M.M., Z.S.N. and P.J.T. conceived and initiated the project. M.M. and Z.S.N. developed the oligocortical spheroid protocol and generated spheroids for all experiments. M.M., H.E.S. B.L.L.C., K.C.A. and L.B. performed immunohistochemistry and quantification and generated associated figures. D.C.F. and B.L.L.C. analyzed RNAseq data and generated associated figures. E.G., C.C-P., and R.H.M. designed and performed electron microscopy experiments and analysis and generated associated figures. H.E.S. maintained pluripotent stem cell lines. T.J., P.D., and V.F. independently replicated the oligocortical spheroid protocol. Z.S.N., M.M., and P.J.T. wrote the manuscript with input from all authors.

Competing Interests

P.J.T. and R.H.M. are consultants for Convelo Therapeutics, which has licensed patents from Case Western Reserve University. P.J.T., R.H.M., and Case Western Reserve University hold equity in Convelo Therapeutics. D.C.F. became an employee of Convelo Therapeutics subsequent to completion of these studies. P.J.T. is a consultant and on the Scientific Advisory Board of Cell Line Genetics. P.J.T. is Chair of the Scientific Advisory Board (volunteer position) for the Pelizaeus-Merzbacher Disease Foundation. All other authors have no competing interests.

provide a versatile platform to observe and dissect the complex interactions required for myelination of the developing central nervous system and offer new opportunities for disease modeling and therapeutic development in human tissue.

INTRODUCTION

Advances in the generation of 3-dimensional (3D) tissues *in vitro* are improving the ability to study human neurodevelopment and disease[1–14]. Human pluripotent stem cell-derived 3D cultures—called "organoids" or "spheroids"—recapitulate complex developmental processes, cell-cell interactions, microenvironments, tissue architectures, and extended temporal dynamics that are inaccessible in traditional *in vitro* cultures[15, 16]. Multiple groups have developed protocols to model the coordinated rounds of cell proliferation, migration, organization, and maturation required to pattern the human cerebral cortex[1, 3, 17]. These pluripotent stem cell-derived "cortical spheroids" have been shown to generate multiple cortical cell types—including neural progenitors, mature neuron subtypes, and astrocytes—self-organize into distinct cortical layers, and establish functional neural networks[1–4, 7–12, 17, 18]. However, while single-cell analyses of cortical spheroids have identified transcriptional profiles suggesting the presence of oligodendrocyte progenitor cells (OPCs)[7, 10], and rare oligodendrocytes have been identified in isolation[19], no protocol has yet demonstrated reproducible generation and maturation of oligodendrocytes, the myelinating glia of the central nervous system (CNS) and the third major cell type of neural origin.

RESULTS

Generation of oligocortical spheroids

We generated OPCs and myelinating oligodendrocytes in human pluripotent stem cell-derived cortical spheroids by timed exposure to defined oligodendrocyte lineage growth factors and hormones. To start, we generated and patterned "neurocortical spheroids" using an optimized version of a 50 day protocol[3]. After initial neurocortical patterning, we generated "oligocortical spheroids" by treatment with platelet-derived growth factor-AA (PDGF-AA) and insulin-like growth factor-1 (IGF-1) to drive the expansion of native OPC populations (days 50–60 = "week 9"), followed by thyroid hormone (T3) to induce oligodendrocyte differentiation, and ultimately myelination (days 60–70 = "week 10") (Fig. 1a). PDGF-AA and IGF-1 are requisite developmental mitogens that promote the proliferation and survival of OPCs[20, 21], and T3 has been shown to regulate and induce the generation of oligodendrocytes from OPCs *in vivo*[22]. Treatment time periods were empirically determined, but mirror the initial specification of OPCs and oligodendrocytes in the human fetal brain at 10 and 14 weeks post-conception, respectively[23, 24].

To assess inter-line variability and demonstrate the robustness of our protocol, we initially developed our protocol using human embryonic stem cell line H7 (female). We then reproduced key experiments using two additional independent human pluripotent cell lines: embryonic stem cell line H9 (female) and in-house derived induced pluripotent stem cell (iPSC) line CWRU191 (male).

Induction of OPCs and oligodendrocytes in oligocortical spheroids

By the end of neurocortical patterning at week 8, neurocortical spheroids contained few cells in the oligodendrocyte lineage as evidenced by minimal immunostaining of OLIG2 and SOX10, two canonical OPC transcription factors (Supplementary Fig. 1b–c). However, subsequent treatment of patterned spheroids with PDGF-AA and IGF-1 for 10 days, resulted in a substantial increase in the number of OPCs within the oligocortical spheroids compared to age-matched untreated neurocortical spheroids (Supplementary Fig. 1c–e).

By week 14, neurocortical spheroids had generated robust populations of neurons and astrocytes, but no oligodendrocytes (Fig. 1b), while oligocortical spheroids (treated with PDGF-AA/IGF-1 from days 50–60 and T3 from days 60–70) reproducibly generated robust populations of oligodendrocytes across all three pluripotent stem cell lines, as demonstrated by immunofluorescence for proteolipid protein 1 (PLP1), the most abundant oligodendrocyte membrane protein, and MYRF[25], a transcription factor specifically expressed in oligodendrocytes in the CNS (Fig. 1c; Supplementary Fig. 2a–c). Importantly, oligocortical spheroids exhibited low inter-line and inter-spheroid variability in the production of MYRF-positive oligodendrocytes: 21.59% ± 4.9%, 20.53% ± 3.9%, and 18.4%± 2.2% of total cells (see Supplementary Fig. 2c for quantification schematic) for H7, H9, and CWRU191 derived oligocortical spheroids, respectively, with n=5 spheroids per line (Fig. 1d). Additionally, robust induction of the oligodendrocyte lineage was dependent on sequential treatment with both PDGF-AA/IGF-1 and T3, as few MYRF-positive oligodendrocytes were produced by either treatment individually (Fig. 1d). Thus, while neurocortical patterning establishes the structural and cellular framework for oligodendrogenesis, PDGF-AA, IGF-1, and T3 are necessary for reproducible induction of OPCs and oligodendrocytes.

To further validate the reproducibility of our approach, the protocol was replicated in an independent laboratory using an independent human pluripotent cell line, human embryonic stem cell line RUES1 (male)[26], and separate personnel and reagents, wherein MYRF-positive cells constituted 18.36% ± 3.37% of cells in RUES derived oligocortical spheroids (Fig. 1d; Supplementary Fig. 2a–b).

Lastly, RNA sequencing of bulk spheroids was used to globally assess how PDGF-AA/IGF-1 and T3 treatments affected transcription of neuron, astrocyte, and oligodendrocyte genes in oligocortical spheroids as compared to age-matched neurocortical spheroids. Analysis of week 14 spheroids for the expression of the 100 most specific mRNA transcripts for each cell type (defined using mouse transcriptional data from brainrnaseq.org[27]) demonstrated no significant changes in neuronal gene sets, but showed a significant upregulation of glial gene sets, in particular those of the oligodendrocyte lineage (Fig. 1e,f). These data demonstrate the method to generate oligocortical spheroids activates a global oligodendrocyte transcriptional program, but does not overtly alter the expression programs of other cell types in the spheroids, including neurons.

Oligodendrocyte maturation and myelination in oligocortical spheroids

After initial oligocortical patterning, spheroids can be maintained in basal media for weeks to months, allowing intrinsic cellular programs to drive further cellular and structural maturation. We analyzed neuronal diversity and oligodendrocyte maturation at weeks 20 and 30 (Fig. 2a). Initial analysis at week 20 demonstrated a relatively immature spheroid. In addition to MYRF-positive oligodendrocytes, week 20 oligocortical spheroids contained a large population of early born deep layer neurons marked by CTIP2 and a separate smaller population of late born superficial layer neurons marked by SATB2, with MYRF-positive oligodendrocytes distributed throughout (Fig. 2b; Supplementary Fig. 3a). However, the neuron populations demonstrated substantial overlap consistent with ongoing migration of younger SATB2 cells through the deep layers.

As oligodendrocytes mature, they extend cellular processes that track and myelinate adjacent axons. While PLP1 expression was robust as early as 14 weeks in culture, PLP1 immunofluorescence did not resolve into distinct processes until week 20 (Fig. 2c; Supplementary Fig. 3a). Furthermore, a subset of these processes began to express myelin basic protein (MBP, Fig. 2d), a marker of early myelin formation, suggesting oligodendrocyte processes were associating with neuronal axons[28]. Analysis of week 20 oligocortical spheroids using electron microscopy (EM) revealed concentric, but often unorganized, wrapping of human axons with multiple layers of uncompacted myelin (Fig. 2e–g; Supplementary Fig. 3b). While the unorganized nature of this early oligocortical spheroid myelin may be attributed, in part, to the *in vitro* culture environment, it does show striking resemblance to the earliest stages of *in vivo* fetal myelinogenesis in both human and chick[29, 30]. Importantly, despite T3 treatment and extensive oligodendrocyte maturation, week 20 oligocortical spheroids also maintained a pool of SOX10-positive, MYRF-negative OPCs (Supplementary Fig. 3c).

After an additional two months in culture, analysis at week 30 revealed CTIP2- and SATB2-marked neuron populations organized into distinct cortical layers, with a large SATB2 population and a smallerCTIP2 layer. MYRF-positive oligodendrocytes were present both throughout these layers and as a distinct layer adjacent to CTIP2. (Fig. 2h). Additionally, oligodendrocyte processes had further resolved into distinct PLP1-positive tracts that co-localized with neurofilament-expressing neuronal axons (Fig. 2i–j). EM at week 30 identified neuronal axons encircled by compact myelin (Fig. 2k), and serial block face imaging with 3D reconstruction demonstrated longitudinal wraps of myelin ensheathing the axon (Figure 2l). However, as of week 30 we could not identify definitive evidence of further structural organization, such as nodes of Ranvier, likely due in part to the continued immaturity and minimal coherent electrical activity of spheroid neurons (a noted issue with all current spheroid and organoid technologies). Collectively, these results demonstrate that early myelination of human neurons by human oligodendrocytes can be generated in the context of oligocortical spheroids in as little as 20 weeks, with myelin maturation, refinement, and compaction by 30 weeks. This *in vitro* timing is similar to the emergence of myelin in the latter part of the third trimester of human fetal development *in utero*[24], as well as the timing of human OPC maturation and myelination after transplantation to the rodent

CNS[31, 32], suggesting the potential presence of a cell-intrinsic developmental clock for human oligodendrocyte maturation as proposed in rodents[33–35].

Relevance to *in vivo* cortical development and organization

We next evaluated the developmental and cellular organization within our oligocortical spheroids to demonstrate relevance to *in vivo* human cortical development. By week 8, spheroids contained robust populations of dividing Nestin-positive and SOX2-positive neural progenitors, organized into SOX2-positive ventricular-like and TBR2-positive outer subventricular-likes zones (Fig. 3a,b). The arrangement of SOX2-positive germinal centers was reminiscent of the ventricular zone in the cortex, although not all SOX2 populations surrounded a ventricle-like void and many were localized to the outer surface of the spheroid. At week 9, we labelled proliferating Sox2-positive cells of these germinal centers with the thymidine analog 5-bromo-2'-deoxyuridine (BrdU) (Fig. 3c and Supplementary Fig. 4a) and tracked the developmental trajectories of these cells. By week 14, BrdU labelled cells had migrated away from the germinal center, forming a distinct population from the SOX2-positive germinal zones (Fig. 3d–e and Supplementary Fig. 4a). At this time point, only oligocortical spheroids contained MYRF-positive OPCs, some of which were MYRF/BrdU-double positive (Fig. 3e and Supplementary Fig. 4a). MYRF co-localization with BrdU is strong evidence that these cells originated from BrdU labeled SOX2-positive progenitors found in progenitor zones of the oligocortical spheroids.

The migration of BrdU-pulsed progenitors away from germinal centers suggests that oligocortical spheroids contain a continuum of proliferative and differentiating oligodendrocytes. To assess the global diversity of cellular composition and spectrum of glial maturation, we performed single cell RNAseq on week 12 oligocortical spheroids—an early time point just after PDGF-AA/IGF-1 and T3 treatment when all populations should be represented. Cell clustering broadly distinguished between glial and neuronal populations. The glial cluster contained early progenitors (marked by vimentin, SOX2, and nestin), OPCs (marked by SOX6), and maturing oligodendrocytes (marked by PLP1 and oligodendrocyte myelin glycoprotein) with expression of proliferative markers throughout the cluster and maturation markers defining progressively more distinct sub-populations (Supplementary Fig. 5a). This single cell analysis demonstrates that distinct populations of oligodendrocytes at multiple stages of development coexist in oligocortical spheroids, similar to single cell transcriptome datasets from human fetal cortex (Supplementary Fig. 5a)[36]. This suggests that oligocortical spheroids might provide an avenue to interrogate these largely inaccessible stages of human glial development.

Oligocortical spheroids provide platform to test promyelinating drugs

The ability to generate human oligodendrocytes that can myelinate human axons in an *in vitro* system provides new opportunities to explore human myelin development, disease, and therapeutics. To first validate the utility and biological relevance of our new human oligocortical spheroid system, we tested whether they recapitulate known effects of previously identified promyelinating drugs. Our group and others have shown two FDA-approved drugs, clemastine and ketoconazole, to be potent stimulators of rodent oligodendrocyte generation and myelination *in vitro* and *in vivo*[37, 38]. Moreover, clemastine

was recently reported to enhance remyelination in a Phase 2 repurposing clinical trial in multiple sclerosis patients[39, 40]. To assess the effect of these promyelinating drugs on human oligodendrocyte generation, oligocortical spheroids were treated with PDGF-AA/IGF-1 from day 50–60, and then either DMSO, T3, clemastine, or ketoconazole from day 60–70, followed by a return to basal medium for 4 weeks. Quantification of MYRF-positive oligodendrocytes at week 14 revealed that clemastine (18.7% ± 2.94%) and ketoconazole (27.61% ± 5.941%) each enhanced the production of oligodendrocytes to a similar extent as T3 (21.59% ± 4.9%), compared to vehicle (DMSO) controls (6.345% ± 1.46%) (Fig. 4a–e). Remarkably, when examined by EM, ketoconazole-treated spheroids also demonstrated myelination by week 14 of culture, two months earlier than T3 treated spheroids (Fig. 4f–g). These results demonstrate that clemastine and ketoconazole enhance and accelerate human oligodendrogenesis and maturation and validate that oligocortical spheroids provide a physiologic and species relevant preclinical model to evaluate candidate myelin therapeutics prior to human clinical trials.

Oligocortical spheroids recapitulate cellular pathology of a genetic myelin disorder

Oligocortical spheroids provide an unprecedented tissue-like, minimally manipulated system in which to study hitherto inaccessible developmental stages of human myelin and the pathologic processes leading to myelin disease. In order to validate that our system can accurately recapitulate known cellular pathology and dysfunction, we investigated the monogenic leukodystrophy Pelizaeus-Merzbacher disease (PMD [MIM 312080]). PMD is a rare X-linked myelin disease caused by mutations in *PLP1* and subsequent dysfunction in myelin production[41]. Hundreds of *PLP1* mutations have been identified in patients, who in turn present with a spectrum of severity ranging from mild symptoms of motor delay and spasticity to severe hypotonia with mortality in early childhood. We previously generated PMD iPSC-derived oligodendrocytes from a panel of affected male patients[28] using a 2-dimensional (2D) culture system[42] and demonstrated both distinct and convergent cellular phenotypes in individuals with various mutations. Here, we generated oligocortical spheroids from three iPSC lines with different PMD mutations: a deletion of the entire *PLP1* locus, a duplication of the entire *PLP1* locus, and a point mutation in *PLP1* (c.254T>G). Phenotypically, these patients were mildly (deletion), moderately (duplication), and severely (point mutation) affected. To control for both gender and cell type of origin, we simultaneously generated spheroids from a healthy control male iPSC line derived in-house, CWRU198, that expressed MYRF (18.4% ± 2.20%) and PLP1 (Fig. 5a–b) to similar extents as previously described control lines H7, H9, and CWRU191.

In oligocortical spheroids, the abundance of MYRF-positive oligodendrocytes trended with disease severity, while the extent of PLP1 expression correlated with genetic status (Fig. 5c–h). The PLP1 deletion line produced abundant MYRF-positive oligodendrocytes (15.14% ± 1.96%), despite the expected absence of PLP1 (Fig. 5c–d,m). Conversely, the duplication line produced abundant PLP1 signal (Fig. 5e), despite a significant decrease in MYRF-positive oligodendrocytes (11.84% ± 2.27%) compared to CWRU198 (Fig. 5f,m). In previous 2D cultures[28], oligodendrocytes generated from this c.254T>G point mutation showed distinct perinuclear retention of PLP1, which resolved upon chemical modulation of the endoplasmic reticulum stress pathway. Oligocortical spheroids recapitulated this

phenotype, demonstrating frank perinuclear retention of PLP1 (Fig. 5g) and the most severe reduction in MYRF-positive oligodendrocytes (9.69% ± 1.82%) (Fig. 5h,m). Subsequent treatment of point mutation oligocortical spheroids with GSK2656157, an inhibitor of protein kinase R-like endoplasmic reticulum kinase (PERK)[43], improved mobilization of PLP1 away from the endoplasmic reticulum and into oligodendrocyte processes (Fig. 5i) and significantly increased the percentage of MYRF-positive cells (15.04% ± 1.96%) (Fig. 5j,m). Lastly, CRISPR correction of the point mutation to the wild type sequence (Supplementary Fig. 6a–c) in iPSCs prior to oligocortical spheroids generation not only restored PLP1 mobilization into oligodendrocyte processes (Fig. 5k), but also increased the percentage of MYRF-positive oligodendrocytes (17.25 ± 3.22%) back to healthy control levels (Fig. 5l–m) and enabled generation of myelin by 20 weeks in culture (Fig. 5n). The mechanisms underlying the spectrum of PMD genotype-phenotype correlates have not been fully characterized. Current data suggest accumulation of excess (e.g. duplication) or aberrant/misfolded (e.g. missense mutation) PLP1 leads to ER stress, cell death, and severe patient phenotypes, while PLP1 deletion is better tolerated[44], and the dichotomy between cell abundance and PLP1 expression in our oligocortical spheroids aligns with this hypothesis. Pluripotent stem cell-derived brain organoids and cortical spheroids have been previously used to dissect mutation-specific pathologic processes involved in neuronal disorders[2, 45–47]. Having validated our system, we can extend these efforts to a wide variety of myelin diseases and begin to explore patient-specific pathogenesis over the course of oligodendrocyte birth, maturation, myelination, and death.

DISCUSSION

Human corticogenesis is a complex process that requires the coordinated generation, migration, and maturation of distinct populations of cells. While many groups have generated oligodendrocytes through *in vitro* 2D cultures[31, 42] and forced aggregation of differentiating neural cells[48], human pluripotent stem cell-derived 3D cortical spheroids provide a system to harness intrinsic cell fate programs to recapitulate regions of organization and cortical layering present in the developing human brain. These complex, self-organizing spheroids provide new opportunities to both observe and perturb brain development. Here, we have developed and optimized a method to induce oligodendrocyte progenitors and myelinating oligodendrocytes in cortical spheroids by exposure to the oligodendrocyte growth factors PDGF, IGF-1, and T3, while preserving the general organization and regional specification demonstrated in prior neuronal models. Further work is required to refine cortical architecture in these spheroids, but the induction of all major lineages of CNS origin provides a new opportunity to study human cortical development and disease.

In the process of validating our system, we have demonstrated two applications for oligocortical spheroids: genetic disease modeling and preclinical drug screening. These experimental approaches could be applied to many outstanding questions in the myelin disease field, from understanding demyelination in the leukodystrophies to developing remyelination strategies to treat multiple sclerosis. However, potential applications extend well beyond oligodendrocyte disease. With further development and refinement of the technology, this system could also be utilized to explore basic questions in myelin

development, including myelination of different classes of neurons, regulation of myelin compaction, modulation of the size of nodes and internodes, and single-neuron and whole-spheroid electrophysiology. As new spheroid variants modelling specific regions of the brain are developed[6], this will open broad avenues to investigate physiology and development of the brain as a whole. Oligodendrogenesis is a multi-phase process, with regional populations of oligodendrocytes arising, migrating, and maturing at distinct times during embryogenesis. In mammals, ventrally derived oligodendrocytes are among the first population to arise, yet are not required for the proper myelination of the cortex and are mostly replaced by later cortex-derived oligodendrocytes[49]. Even compared to non-human primates, the timing and duration of human myelination is regionally-distinct[50]. Human oligocortical spheroids, now provide an accessible system to explore these and many other uniquely human aspects of myelin development.

ONLINE METHODS

Pluripotent stem cell lines.

Healthy (CWRU191; CWRU198) and PMD iPSCs were generated previously after informed consent and approval of the Case Western Reserve University and University Hospital Institutional Review Board [28, 51]. Two human embryonic stem cell (hESC) lines from the approved NIH hESC Registry (“H7” NIHhESC-10–0061; “H9” NIHhESC-10–0062) were also used in these studies.

Oligocortical Spheroid Differentiation.

Neurocortical spheroids were generated from human pluripotent stem cells as previously described with variations noted below[3].

To pattern neurocortical spheroids, pluripotent stem cell colonies cultured on vitronectin (Gibco #A14700) were lifted using dispase (Gibco #17105–041) at 37°C for 10 minutes. Intact colonies were transferred to individual low-adherence V-bottom 96-well plates (S-Bio Prime #MS-9096VZ) in 200μl Spheroid Starter media with 10μM Rock inhibitor Y-27632 (Calbiochem #688001), 10 μM Dorsopmorphin (Sigma #P5499), and 10 μM SB-431542 (Sigma #S4317). Spheroid Starter media was DMEM/F12 (Invitrogen #11320–033) containing 20% Knock out Serum (Invitrogen #12587–010), Non-essential amino acids (Invitrogen #11140050), Glutamax (Invitrogen #35050061), β-mercaptoethanol and 100U/ml Penicillin/Streptomycin. The same media without rock inhibitor was used for the next five days, after which the media was changed to Neurobasal-A based spheroid media. Neurobasal-A spheroid media was Neurobasal-A medium (Invitrogen #10888022) with added B-27 serum substitute without vitamin A (Invitrogen #12587), Glutamax (Invitrogen #35050061) and 100U/ml Penicillin/Streptomycin. From day 7–25, 20ng/ml FGF-2 (R&D systems #233-FB-25/CF) and 10ng/ml EGF (R&D systems #236-EG-200) were added to the media. Spheroids were cultured in 96-well plates through day 25, with daily half-media changes. On day 25, spheroids were transferred to ultra-low attachment 6-well plates (Corning #CLS3471) at a density of 8–10 spheroids per well and cultured thus through the remainder of the protocol. Also from this point forward 1% Geltrex (Invitrogen # A15696–01) was added to the Neurobasal-A spheroid media. Neural differentiation was induced

between days 27 and 41 by supplementing Neurobasal-A spheroid media with 20ng/ml BDNF (R&D systems #248-BD) and 20ng/ml NT-3 (R&D systems #267-N). Half media changes were performed every other day between days 17 and 41.

To generate oligocortical spheroids, beginning on day 50, 10 ng/ml platelet-derived growth factor-AA (PDGF-AA, R&D Systems #221-AA-050) and 10 ng/ml insulin-like growth factor-1 (IGF-1, R&D Systems #291-G1–200) were added to the every-other-day media changes for 10 days. Next, on day 60, 40 ng/ml 3,3',5-triiodothronine (T3, Sigma #ST2877) was added to the every-other-day media changes for 10 days. When used, small molecules were supplemented during this period. 4μM Ketoconazole and 2 μM Clemastine were added in lieu of T3. GSK2656157 was added in addition to T3.

After day 70, spheroids were matured and maintained in Neurobasal-A spheroid media with every-other-day media changes until completion of the experiment.

Independent Validation.

One hESC line "RUES1" from the approved NIH hESC Registry (NIHhESC-09–0012) was used. RUES1 were cultured on matrigel in mTeSR1 medium (Stemcell Technologies #85850) and lifted using StemPro Accutase (Thermofisher #A1110501). Oligocortical spheroid differentiation was performed as described above, with the exception of using N2 supplement (Thermofisher #17502048) and 25mg/ml human insulin solution (Sigma #I9278) in replacement of KSR for days 1–7 of the differentiation protocol.

Small Molecules.

4mM stock solution of Ketoconazole (Sigma #K1003), 2mM stock solution of Clemastine fumarate (Sigma #SML0445), and 10mM stock solution of GSK2656157 (EMD Millipore #5046510001) were prepared, aliquoted, and stored at −20°C. Small molecules were warmed to 37°C for 20 minutes before adding to pre-warmed medium. Frozen aliquots were thawed no more than twice before being discarded.

BrdU Labeling.

To label dividing cells in the spheroid, BrdU was added to culture media at a final concentration of 3μg/ml on day 58 and day 60. Week 9 samples were collected 4 hours after BrdU administration on day 60. For lineage tracing experiments, BrdU labelled spheroids were collected on week 14 and processed for immunohistochemistry.

PLP1 Gene Editing.

CRISPR-Cas9 editing of a *PLP1* point mutation (c.254T>G) in iPSCs was performed by the Genome Engineering and iPSC Center at Washington University in St. Louis using a guide RNA overlapping the mutation (sequence: CCAGCAGGCGGGCCCCATAAAGG) and a single strand oligonucleotide with 25 nucleotide homology arms surrounding the mutation. Upon receipt, the mutation and correction locus were resequenced and both lines were karyotyped to ensure no gross genotypic aberrations were generated during the editing process (Cell Line Genetics).

Immunocytochemistry.

Spheroids for immunohistochemistry were initially fixed with 4% ice-cold paraformaldehyde for 45 minutes, washed three times in PBS, and equilibrated with 30% sucrose overnight. The spheroids were embedded in OCT and sectioned at 10μm.

Immunohistochemistry was performed as described previously[52]. Briefly, sections were washed in PBS three times and then blocked for 30 minutes in PBS containing 0.1% Triton X-100 and 0.25% Normal donkey serum. The sections were then incubated at 4°C overnight using primary antibodies in blocking solution. Primary antibodies used: rat-anti-PLP1 (1:500, AA3, gift from Wendy Macklin); rabbit-anti-MYRF (1:1000, provided by Dr. Michael Wegner); goat anti-SOX10 (1:250 R&D Systems AF 2864); rabbit anti-OLIG2 (1:250, Millipore AB9610; mouse-anti-pan-axonal neurofilament (1:1000, Covance #SMI311); mouse-anti-MBP (1:200, Covance # Smi99), mouse-anti-pan-neuronal neurofilament (NF, 1:1000, Covance #SMI312); rabbit-anti-GFAP (1:1000, Dako #Z0334); mouse anti-SATB2 (1:250, Abcam, #ab51520); rat anti-CTIP2 (1:400, Abcam #ab18465); goat anti-SOX2 (1:250 R&D Systems, #AF2018); rabbit anti-TBR2 (1:250, Abcam, ab23345); mouse anti-Ki67 (1:250, Millipore MAB4190); mouse anti-Nestin (1:1000 Millipore, MAB5326); mouse anti-BrdU (1:1000, Millipore, MAB3510); chicken anti-Vimentin (1:1000 Abcam, ab24525); DAPI (1ug/ml, Sigma #D8417). Sections were then washed in PBS and incubated in secondary antibodies for 2 hours. All secondary antibodies were LifeTechnologies AlexaFluor conjugated secondary antibodies used at a dilution of 1:500. In the case of PLP1 immunohistochemistry, a 20 minute wash in PBS containing 10% Triton X-100 was first performed prior to the blocking step. In the case of MBP immunohistochemistry, a 20 minute ice cold acetone post fixation step was used. BrdU immunohistochemistry was performed after antigen retrieval, which entailed placing slides in a sealed coplin jar with boiling 100mM Sodium Citrate Buffer and allowing it to come to room temperature over the course of an hour.

Spheroid sections were imaged using either a Leica DMi8 fluorescence microscope or a Leica Sp8 confocal microscope at the Case Western Reserve School of Medicine Imaging Core. In order to count MYRF positive nuclei, four 20X fields were imaged per spheroid. Two fields from the top and bottom of the spheroid and 2 fields from the edges of the central region of the spheroids were quantified (see Supplementary Fig. 1c for schematic). The total number of DAPI-positive cells and MYRF-positive cells were manually counted in Adobe Photoshop or NIH ImageJ. Three to five spheroids were analyzed per line and treatment condition and Graphpad Prism was used to perform a t-test to assess statistical significance between lines or treatments.

Electron Microscopy.

Spheroids were fixed and processed as previously described[52]. Samples were fixed for 1 hour at room temperature in a fixative solution containing 4% Paraformaldehyde (EMS), 2% Glutaraldehyde (EMS), and 0.1M Na Cacodylate (EMS). Samples were then osmicated, stained with uranyl acetate and embedded in EMbed 812 (EMS). Ultrathin sections (120 nm) from each spheroid sample were observed with a FEI Helios NanoLab™ 660 FIBSEM using extreme high resolution (XHR) field emission scanning electron microscope equipped

with a Concentric (insertable) higher energy electron detector, all images were taken using 4 Kv and 0.2 current landing voltage at high magnifications (15000–35000x).

Serial Block Face Imaging and 3D-Reconstruction.

Epoxy embedded spheroids were trimmed, mounted onto silicon wafers and covered by conductive silver paint. Using a sputter coating (Cressington Scientific Instruments) an additional iridium layer ~1nm was deposited and samples were loaded into a Helios Nanolab 660i dual beam microscope (FEI Company) for imaging. After setting up the ion column and beam coincidence at the eucentric height (tilt 52°), for electron beam 2 kV and 40 pA current landing was used, then ion beam (Ga+) assisted platinum was deposited as a protective layer for subsequent milling for cross section using low current 0.23 nA, while surplus block material was removed using a high ion beam current (30 kV, 6.5 nA). For final surface polishing/milling, a reduced ion current was used (30 KV, 2.8 nA). For imaging, the Auto Slice and View G3 software (FEI Company) was used with an electron beam current of 400 pA, HFW 11.84 um, to acquire an image stack of 154 sections (pixel size: 1.97, and z = 50nm) using TLD detector, with a resolution of 6144 × 4096, dwell time 6μs, working distance 4.04 mm. Raw images were aligned in Fuji imaging processing package and Imaris 9.1 software (Bitplane AG) was used for image visualization and 3D-reconstruction of myelin bundle.

Bulk RNA Sequencing and Analysis.

Four spheroids per line were collected in TriReagent (Zymo Research #R2050–1-200) and RNA was extracted as per manufacturer's instructions. RNA was further purified using a Qiagen RNeasy Plus Mini kit (Qiagen, #73404). Illumina libraries were prepared and sequenced in 50bp paired end mode on a HiSeq 2500 instrument at the CWRU Genomics Core facility. Reads were aligned to the hg19 genome using TopHat v2.0.6 without providing a reference transcriptome[53]. Abundance of transcripts from the iGenomes hg19 RefSeq reference were measured using Cufflinks v2.0.2[54]. FPKMs were quantile normalized. Neuron-, astrocyte- and oligodendrocyte-specific genes were defined by expression (FPKM>1) in their respective cells and absence in the other two lineages[27]. Each list was reduced to the 100 genes most specific to that cell-type by fold-change that were also detected in at least one spheroid sample. Differences in expression of gene lists were assessed using the Wilcoxon test in Graphpad Prism.

Single Cell RNA Sequencing and Analysis.

Ten independently generated week 12 spheroids were pooled and dissociated as previously described[55]. Briefly, spheroids were dissociated using the Worthington Papain dissociation system (Worthington Biochemical Corp., Lakewood NJ, Cat#: LK003150) following the manufacturer's instructions. Papain solution was oxygenated with 95% O2 and 5% CO2 prior to dissociation. Cell counts of single cell suspension were performed on the Countess Automated Cell Counter (Invitrogen) and cells were loaded for single cell capture at a final concentration of 1,000 cells/ul.

Single cell capture, cDNA synthesis, cDNA preamplification, and library preparation were performed using the 10x Genomics Chromium Single Cell 3' Library and Bead Kit v2 (10x

Genomics Inc, Pleasanton CA, Cat#: 120237). 3,850 cells were recovered and sequenced at a depth of 38,611 reads per cell with 1,870 median genes per cell. Cell Ranger Single-Cell Software Suite v2.1.0 was used for barcode processing and single-cell 3' gene counting and reads were mapped to hg19. PCA dimensionality reduction and tSNE analysis was performed by Cell Ranger Single-Cell Software Suite v2.1.0 and data visualized using 10x Genomics Loupe Cell Browser v2.0.0. Data in Figure 2 was clustered with 10x Genomics Loupe Cell Browser v2.0.0 using K-Means clustering with a present number of 2 clusters to isolate broad clusters of neuronal and glial/progenitor. Clustering of spheroids was compared to publically available single-cell data from developing human cortex and available on UCSC Cluster Browser (bit.ly/cortexSingleCell)[36]. Oligocortical spheroid gene expression cluster heatmaps in Figure 2 were generated by 10x Genomics Loupe Cell Browser v2.0.0 and represent the Log2Fold change of gene expression in each cell compared to the mean expression of that gene in the population as a whole. Comparative gene expression cluster heatmaps of developing human cortex were generated from the UCSC Cluster Browser.

Life Sciences Reporting Summary.

Further information on experimental design is available in the Life Sciences Reporting Summary.

Data availability.

All RNA-seq data have been deposited to the Gene Expression Omnibus (GEO) database under the accession number GSE110006. The datasets generated and analyzed during the current study are available from the corresponding author on reasonable request.

Statistics.

In order to quantify the percentage of MYRF positive oligodendrocytes in a single spheroid, 4 regions (as shown in supplementary figure 2) were imaged and the percentage of MYRF cells were averaged per spheroid. For data shown in Figure 1, five spheroids (n=5) were analyzed similarly per treatment group. For data shown in Figure 4, four spheroids were analyzed in each group (n=4). Data presented in Figure 5m, was obtained from five (n=5) spheroids of line CWRU 198 and four spheroids from each PMD line (n=4). A two tailed unpaired t-test with Welch's correction was performed to compare 2 groups at a time.

Bulk RNAseq was performed using 5 spheroids from each condition. Paired non-parametric Wilcoxon matched pairs signed-rank test was used to determine statistical significance.

Supplementary Material

Refer to Web version on PubMed Central for supplementary material.

Acknowledgements

This research was supported by grants from the NIH R01NS093357 (P.J.T.), R01NS095280 (P.J.T. and R.H.M.), T32GM007250 (Z.S.N.) and F30HD084167 (Z.S.N.); the Pelizaeus-Merzbacher Disease Foundation (P.J.T.); the New York Stem Cell Foundation (P.J.T.); the Connor B. Judge Foundation (P.J.T); the New York Stem Cell Foundation Research Institute (V.F.); the National Stem Cell Foundation (T.J. and V.F.); and philanthropic support

from the Peterson, Fakhouri, Long, Goodman, Geller, Galbut/Heil, and Weidenthal families. VF is supported by The New York Stem Cell Foundation Research Institute and TJ was supported by the National Stem Cell foundation Additional support was provided by the CWRU SOM Light Microscopy Core Facility (S10-OD016164) and the Genomics core facility of the Case Comprehensive Cancer Center (P30CA043703). We are grateful to B. Nawash, C. Blake, M. Cartwright, M. Cameron, R. Lee, A. Miron, S. Edelheit, M. Hitomi, F. Pirozzi, and A. Wynshaw-Boris for technical assistance and discussion.

REFERENCES

1. Kadoshima T et al. Self-organization of axial polarity, inside-out layer pattern, and species-specific progenitor dynamics in human ES cell-derived neocortex. Proc Natl Acad Sci U S A 110, 20284–20289 (2013). [PubMed: 24277810]
2. Lancaster MA et al. Cerebral organoids model human brain development and microcephaly. Nature 501, 373–379 (2013). [PubMed: 23995685]
3. Pasca AM et al. Functional cortical neurons and astrocytes from human pluripotent stem cells in 3D culture. Nat Methods 12, 671–678 (2015). [PubMed: 26005811]
4. Camp JG et al. Human cerebral organoids recapitulate gene expression programs of fetal neocortex development. Proc Natl Acad Sci U S A 112, 15672–15677 (2015). [PubMed: 26644564]
5. Jo J et al. Midbrain-like Organoids from Human Pluripotent Stem Cells Contain Functional Dopaminergic and Neuromelanin-Producing Neurons. Cell Stem Cell 19, 248–257 (2016). [PubMed: 27476966]
6. Bagley JA, Reumann D, Bian S, Levi-Strauss J & Knoblich JA Fused cerebral organoids model interactions between brain regions. Nat Methods 14, 743–751 (2017). [PubMed: 28504681]
7. Birey F et al. Assembly of functionally integrated human forebrain spheroids. Nature 545, 54–59 (2017). [PubMed: 28445465]
8. Lancaster MA et al. Guided self-organization and cortical plate formation in human brain organoids. Nat Biotechnol (2017).
9. Li Y et al. Induction of Expansion and Folding in Human Cerebral Organoids. Cell Stem Cell 20, 385–396 e383 (2017). [PubMed: 28041895]
10. Quadrato G et al. Cell diversity and network dynamics in photosensitive human brain organoids. Nature 545, 48–53 (2017). [PubMed: 28445462]
11. Renner M et al. Self-organized developmental patterning and differentiation in cerebral organoids. EMBO J (2017).
12. Sloan SA et al. Human Astrocyte Maturation Captured in 3D Cerebral Cortical Spheroids Derived from Pluripotent Stem Cells. Neuron 95, 779–790 e776 (2017). [PubMed: 28817799]
13. Xiang Y et al. Fusion of Regionally Specified hPSC-Derived Organoids Models Human Brain Development and Interneuron Migration. Cell Stem Cell 21, 383–398 e387 (2017). [PubMed: 28757360]
14. Nakano T et al. Self-formation of optic cups and storable stratified neural retina from human ESCs. Cell Stem Cell 10, 771–785 (2012). [PubMed: 22704518]
15. Pasca SP The rise of three-dimensional human brain cultures. Nature 553, 437–445 (2018). [PubMed: 29364288]
16. Arlotta P Organoids required! A new path to understanding human brain development and disease. Nat Methods 15, 27–29 (2018). [PubMed: 29298289]
17. Lancaster MA & Knoblich JA Generation of cerebral organoids from human pluripotent stem cells. Nat Protoc 9, 2329–2340 (2014). [PubMed: 25188634]
18. Luo C et al. Cerebral Organoids Recapitulate Epigenomic Signatures of the Human Fetal Brain. Cell Rep 17, 3369–3384 (2016). [PubMed: 28009303]
19. Monzel AS et al. Derivation of Human Midbrain-Specific Organoids from Neuroepithelial Stem Cells. Stem Cell Reports 8, 1144–1154 (2017). [PubMed: 28416282]
20. McMorris FA, Smith TM, DeSalvo S & Furlanetto RW Insulin-like growth factor I/somatomedin C: a potent inducer of oligodendrocyte development. Proc Natl Acad Sci U S A 83, 822–826 (1986). [PubMed: 3511475]

21. Noble M, Murray K, Stroobant P, Waterfield MD & Riddle P Platelet-derived growth factor promotes division and motility and inhibits premature differentiation of the oligodendrocyte/type-2 astrocyte progenitor cell. Nature 333, 560–562 (1988). [PubMed: 3287176]
22. Barres BA, Lazar MA & Raff MC A novel role for thyroid hormone, glucocorticoids and retinoic acid in timing oligodendrocyte development. Development 120, 1097–1108 (1994). [PubMed: 8026323]
23. Jakovcevski I, Filipovic R, Mo Z, Rakic S & Zecevic N Oligodendrocyte development and the onset of myelination in the human fetal brain. Front Neuroanat 3, 5 (2009). [PubMed: 19521542]
24. Silbereis JC, Pochareddy S, Zhu Y, Li M & Sestan N The Cellular and Molecular Landscapes of the Developing Human Central Nervous System. Neuron 89, 248–268 (2016). [PubMed: 26796689]
25. Bujalka H et al. MYRF is a membrane-associated transcription factor that autoproteolytically cleaves to directly activate myelin genes. PLoS Biol 11, e1001625 (2013). [PubMed: 23966833]
26. James D, Noggle SA, Swigut T & Brivanlou AH Contribution of human embryonic stem cells to mouse blastocysts. Dev Biol 295, 90–102 (2006). [PubMed: 16769046]
27. Zhang Y et al. An RNA-sequencing transcriptome and splicing database of glia, neurons, and vascular cells of the cerebral cortex. J Neurosci 34, 11929–11947 (2014). [PubMed: 25186741]
28. Nevin ZS et al. Modeling the Mutational and Phenotypic Landscapes of Pelizaeus-Merzbacher Disease with Human iPSC-Derived Oligodendrocytes. Am J Hum Genet 100, 617–634 (2017). [PubMed: 28366443]
29. Weidenheim KM, Kress Y, Epshteyn I, Rashbaum WK & Lyman WD Early myelination in the human fetal lumbosacral spinal cord: characterization by light and electron microscopy. J Neuropathol Exp Neurol 51, 142–149 (1992). [PubMed: 1538238]
30. Szuchet S, Nielsen LL, Domowicz MS, Austin JR 2nd & Arvanitis DL CNS myelin sheath is stochastically built by homotypic fusion of myelin membranes within the bounds of an oligodendrocyte process. J Struct Biol 190, 56–72 (2015). [PubMed: 25682762]
31. Wang S et al. Human iPSC-derived oligodendrocyte progenitor cells can myelinate and rescue a mouse model of congenital hypomyelination. Cell Stem Cell 12, 252–264 (2013). [PubMed: 23395447]
32. Windrem MS et al. Human iPSC Glial Mouse Chimeras Reveal Glial Contributions to Schizophrenia. Cell Stem Cell 21, 195–208 e196 (2017). [PubMed: 28736215]
33. Gao FB, Durand B & Raff M Oligodendrocyte precursor cells count time but not cell divisions before differentiation. Curr Biol 7, 152–155 (1997). [PubMed: 9016704]
34. Raff MC, Lillien LE, Richardson WD, Burne JF & Noble MD Platelet-derived growth factor from astrocytes drives the clock that times oligodendrocyte development in culture. Nature 333, 562–565 (1988). [PubMed: 3287177]
35. Temple S & Raff MC Clonal analysis of oligodendrocyte development in culture: evidence for a developmental clock that counts cell divisions. Cell 44, 773–779 (1986). [PubMed: 3948247]
36. Nowakowski TJ et al. Spatiotemporal gene expression trajectories reveal developmental hierarchies of the human cortex. Science 358, 1318–1323 (2017). [PubMed: 29217575]
37. Najm FJ et al. Drug-based modulation of endogenous stem cells promotes functional remyelination in vivo. Nature 522, 216–220 (2015). [PubMed: 25896324]
38. Mei F et al. Micropillar arrays as a high-throughput screening platform for therapeutics in multiple sclerosis. Nat Med 20, 954–960 (2014). [PubMed: 24997607]
39. Cohen JA & Tesar PJ Clemastine fumarate for promotion of optic nerve remyelination. Lancet 390, 2421–2422 (2017). [PubMed: 29029894]
40. Green AJ et al. Clemastine fumarate as a remyelinating therapy for multiple sclerosis (ReBUILD): a randomised, controlled, double-blind, crossover trial. Lancet 390, 2481–2489 (2017). [PubMed: 29029896]
41. Hobson GM & Garbern JY Pelizaeus-Merzbacher disease, Pelizaeus-Merzbacher-like disease 1, and related hypomyelinating disorders. Semin Neurol 32, 62–67 (2012). [PubMed: 22422208]
42. Douvaras P et al. Efficient generation of myelinating oligodendrocytes from primary progressive multiple sclerosis patients by induced pluripotent stem cells. Stem Cell Reports 3, 250–259 (2014). [PubMed: 25254339]

43. Axten JM et al. Discovery of GSK2656157: An Optimized PERK Inhibitor Selected for Preclinical Development. ACS Med Chem Lett 4, 964–968 (2013). [PubMed: 24900593]
44. Garbern JY Pelizaeus-Merzbacher disease: Genetic and cellular pathogenesis. Cell Mol Life Sci 64, 50–65 (2007). [PubMed: 17115121]
45. Bershteyn M et al. Human iPSC-Derived Cerebral Organoids Model Cellular Features of Lissencephaly and Reveal Prolonged Mitosis of Outer Radial Glia. Cell Stem Cell 20, 435–449 e434 (2017). [PubMed: 28111201]
46. Mariani J et al. FOXG1-Dependent Dysregulation of GABA/Glutamate Neuron Differentiation in Autism Spectrum Disorders. Cell 162, 375–390 (2015). [PubMed: 26186191]
47. Qian X et al. Brain-Region-Specific Organoids Using Mini-bioreactors for Modeling ZIKV Exposure. Cell 165, 1238–1254 (2016). [PubMed: 27118425]
48. Pamies D et al. A human brain microphysiological system derived from induced pluripotent stem cells to study neurological diseases and toxicity. ALTEX 34, 362–376 (2017). [PubMed: 27883356]
49. Kessaris N et al. Competing waves of oligodendrocytes in the forebrain and postnatal elimination of an embryonic lineage. Nat Neurosci 9, 173–179 (2006). [PubMed: 16388308]
50. Miller DJ et al. Prolonged myelination in human neocortical evolution. Proc Natl Acad Sci U S A 109, 16480–16485 (2012). [PubMed: 23012402]
51. Sheng Y et al. Using iPSC-derived human DA neurons from opioid-dependent subjects to study dopamine dynamics. Brain Behav 6, e00491 (2016). [PubMed: 27547496]
52. Najm FJ et al. Rapid and robust generation of functional oligodendrocyte progenitor cells from epiblast stem cells. Nat Methods 8, 957–962 (2011). [PubMed: 21946668]
53. Trapnell C, Pachter L & Salzberg SL TopHat: discovering splice junctions with RNA-Seq. Bioinformatics 25, 1105–1111 (2009). [PubMed: 19289445]
54. Trapnell C et al. Transcript assembly and quantification by RNA-Seq reveals unannotated transcripts and isoform switching during cell differentiation. Nat Biotechnol 28, 511–515 (2010). [PubMed: 20436464]
55. Marques S et al. Oligodendrocyte heterogeneity in the mouse juvenile and adult central nervous system. Science 352, 1326–1329 (2016). [PubMed: 27284195]

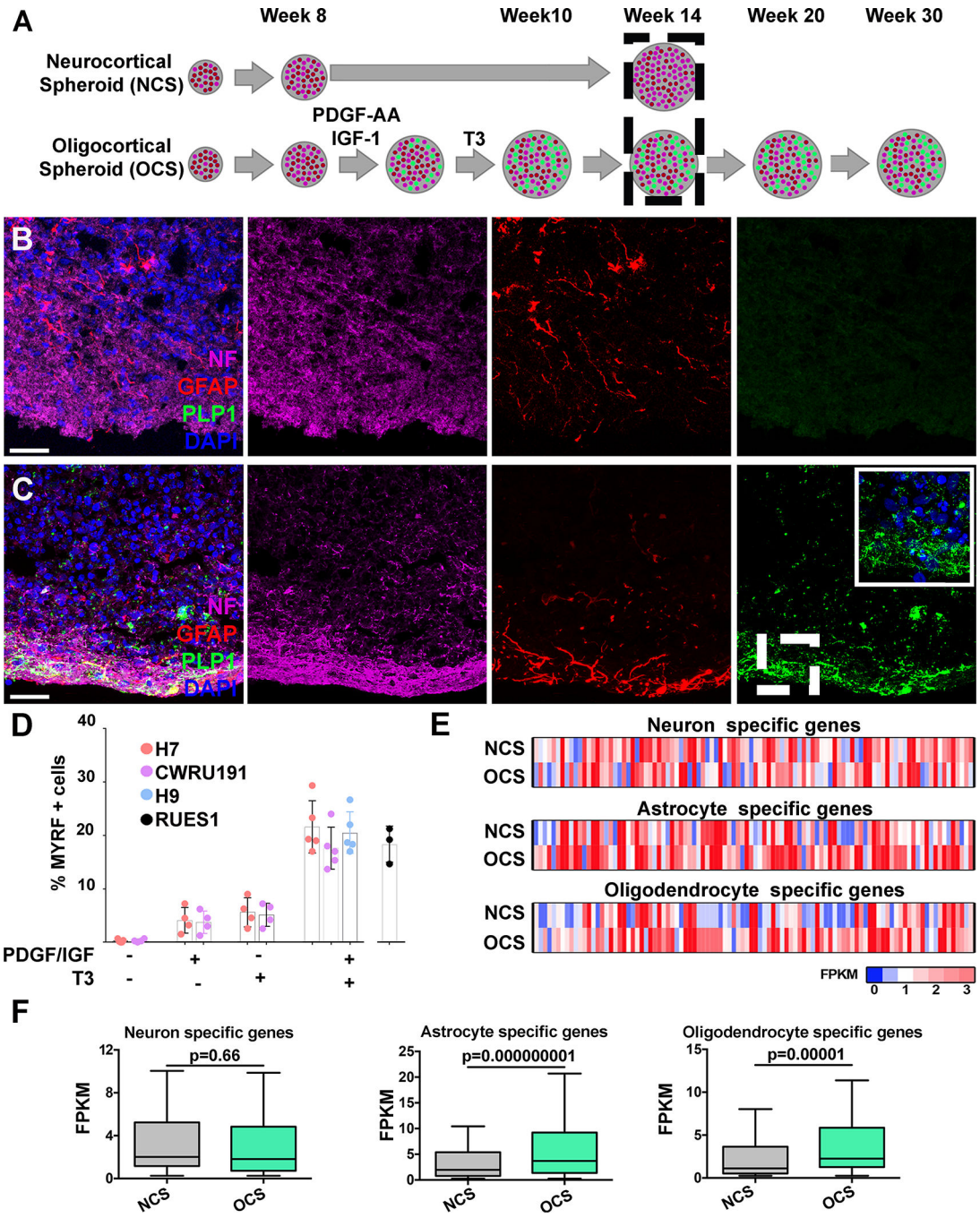

Figure 1 |. Generation of oligodendrocytes in human cortical spheroids.

a, Schematic of spheroid generation. The protocols to generate neurocortical spheroids (NCS) and oligocortical spheroids (OCS) were the same until week 8, after which time neurocortical spheroids were grown in basal media, while oligocortical spheroids were treated with PDGF-AA/IGF-1 from day 50–60 and T3 from day 60–70. Differentiation of oligodendrocytes was assessed at week 14 (dotted box), and these data are presented in Fig. 1. Colors in the schematic simulate neurons (magenta), astrocytes (red) and OPCs/

Oligodendrocytes (green). Maturation of oligodendrocytes was evaluated at weeks 20 and 30, and these data are presented in Fig. 2.

b, Representative fluorescence images of week 14, H7 spheroids generated with the neurocortical protocol. These spheroids generate neurons (Neurofilament:magenta) and astrocytes (GFAP:red), but no oligodendrocytes (PLP1:green). Similar results were obtained from 3 independent batches of spheroids generated from 4 separate lines. Scale bar, 50um.

c, Representative fluorescence images of week 14, H7 spheroids generated with the oligocortical protocol. These spheroids generate neurons (Neurofilament:magenta), astrocytes (GFAP:red), and oligodendrocytes (PLP1:green). Scale bar, 50um. Higher magnification of oligodendrocyte morphology is shown in inset. Representative fluorescence images of H9, CWRU191, and RUES1 spheroids generated with the oligocortical protocol. Similar results were obtained from 3 independent batches of spheroids generated from 4 separate lines. Scale bar, 50um.

d, Quantification of MYRF, a nuclear marker of the oligodendrocyte lineage, in week 14 spheroids generated with the neurocortical or oligocortical protocols as well as with either PDGF-AA and IGF-1 or T3 only. MYRF-positive cells were counted from four planes from four or five individual spheroids (n=4, PDGF/IGF or T3 treatments, n=5, NCS and OCS) for each treatment condition from lines H7, H9 and CWRU191 cell line and averaged (white boxes). Error bars are standard deviation. Three spheroids (n=3) from the same batch were used for the externally validated line RUES1. Representative fluorescence images of MYRF expression in additional lines and a schematic of MYRF quantification are shown in Supplementary Figure 2b–c.

e, RNAseq comparing neuron, astrocyte, and oligodendrocyte gene expression in neurocortical and oligocortical spheroids. The heat maps consist of the 100 most cell specific transcripts for each cell type. Oligodendrocyte as well astrocyte specific genes are upregulated in oligocortical spheroids compared to neurocortical spheroids.

f, Neuron, astrocyte, and oligodendrocyte-specific gene expression from the RNAseq shown in **e**. Box plots display the first and third quartiles, split by the mean; whiskers extend to include the maximum and minimum values. Oligocortical spheroids show a statistically significant change in astrocyte and oligodendrocyte specific gene expression compared to neurocortical spheroids. RNAseq experiment was performed using 5 spheroids from each condition, Paired non-parametric Wilcoxon matched pairs signed-rank test was used to determine statistical significance.

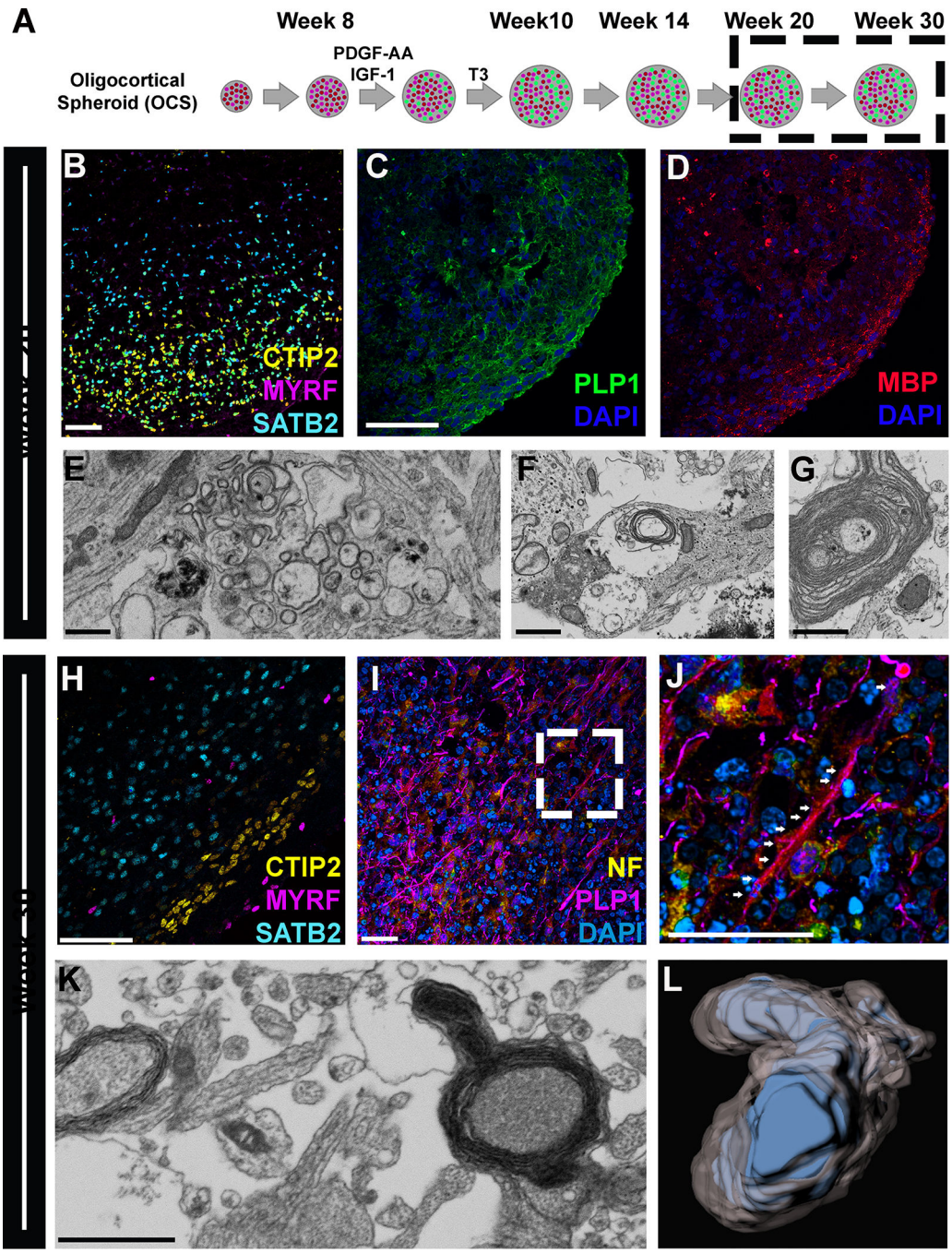

Figure 2 |. Maturation of oligodendrocytes oligocortical spheroids.

a, Schematic depicting the generation of oligocortical spheroids. Colors in the schematic simulate neurons (magenta), astrocytes (red) and OPCs/Oligodendrocytes (green). Maturation of oligodendrocytes was evaluated at weeks 20 and 30 (dotted box), and these data are presented in Fig. 2.

b, Representative fluorescence image of week 20, H7 oligocortical spheroids show robust generation of the oligodendrocyte lineage (MYRF:magenta) as well as early born CTIP2-positive (yellow) neurons and SATB2-positive (cyan) late born neurons. Scale bar, 50um.

Representative fluorescence images of week 20 MYRF expression in additional lines are shown in Supplementary Fig. 3a. Similar results were obtained from 2 independent batches of spheroids.

c, Representative fluorescence image of week 20, H7 oligocortical spheroids demonstrate linear process formation in maturing oligodendrocytes (PLP1:green). Scale bar, 50um for **c** and **d**. Representative fluorescence images of week 20 PLP1 expression in additional lines are shown in Supplementary figure 3. Similar results were obtained from 2 independent batches of spheroids.

d, Representative fluorescence image of week 20, H7 oligocortical spheroids immunostained for MBP (red), a marker of mature myelin, shows punctate MBP expression indicative of an early stage of maturation. Similar results were obtained from 2 independent batches of spheroids.

e, Representative EM of week 20, H7 oligocortical spheroids showing a cluster of neurons that are being myelinated by oligodendrocytes. Scale bar, 1um. EM results were obtained from 3 spheroids from a single batch of spheroids.

f, Representative EM of week 20, H7 oligocortical spheroids shows an axon encircled by multiple layers of loosely compacted myelin. Scale bar, 1um. Representative EMs of myelin in additional lines are shown in Supplementary Fig. 3b. EM results were obtained from 3 spheroids from a single batch of spheroids.

g, Representative EM of week 20, H7 oligocortical spheroids shows more extensive wrapping of loosely compacted myelin encircling an axon. Scale bar, 1um. EM results were obtained from 3 spheroids from a single batch of spheroids.

h, Representative fluorescence image of week 30, H9 oligocortical spheroids shows cortical lamination and separation of CTIP2-positive (yellow) deep layers from SATB2-positive (cyan) superficial layers. MYRF-positive (magenta) oligodendrocytes are interspersed within the cortical layers. Similar results were obtained from 4 spheroids from a single batch of oligocortical spheroids. Scale bar, 50um.

i-j, Representative images of week 30, H9 oligocortical spheroids show oligodendrocyte processes (PLP1:magenta) tracking (arrows) neuron axons (neurofilament:yellow). Higher Magnification images of inset in figure **i** is shown in **j**. Similar results were obtained from 4 spheroids from a single batch of oligocortical spheroids. Scale bar, 50um.

k, Electron micrograph of week 30 H9 oligocortical spheroids showing compact myelin around axons. EM results were obtained from 3 spheroids from a single batch of spheroids Scale bar, 1um.

l, 3D reconstruction from block face EM sections taken along the length of an axon.

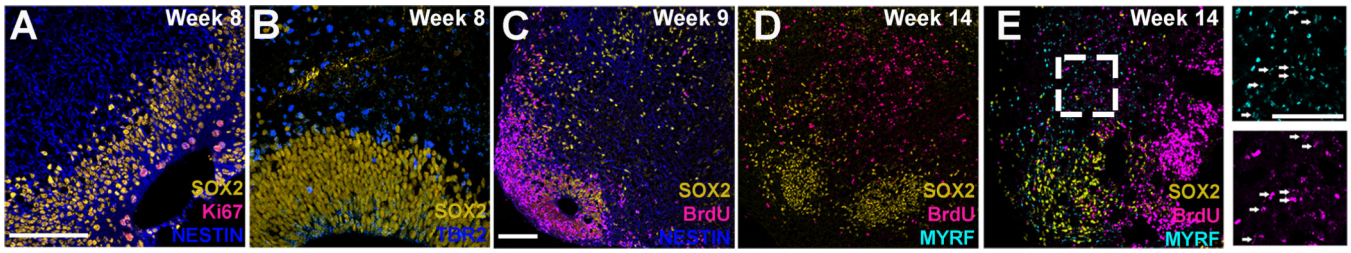

Figure 3 |. Cortical patterning and organization in oligocortical spheroids.

a, Representative fluorescence image of week 8, H7 spheroids at the end of initial neurocortical patterning. These spheroids generate distinct populations of neural progenitors (SOX2:yellow and Nestin:blue) that organize into ventricular-like zones. These cells are also the only actively dividing cells as marked by Ki67 (magenta). Scale bar, 50um for **a** and **b**.

b, Representative Fluorescence image of week 8, H7 spheroids show the presence of a TBR2-positive (blue) outer SVZ-like zone adjacent to the Sox2-positive (yellow) ventricular-like area.

c, Representative fluorescence image of H7 spheroids generated with the oligocortical protocol up through PDGF-AA/IGF-1 treatment, then administered two doses of BrdU (magenta) during week 9 (day 58 and 60) to label dividing cells. BrdU-positive cells localize to SOX2-positive ventricular zones, identifying this as a primary germinal center. Scale bar, 50um for **c-e**.

d-e, Representative fluorescence images of H7 spheroids generated with either the neurocortical (**d**) or oligocortical (**e**) protocol, treated with BrdU during week 9 (Day 58 and 60), and then maintained through week 14. Only oligocortical spheroids generate oligodendrocytes (MYRF:cyan), many of which are double positive for BrdU (arrows in high magnification **inset**).

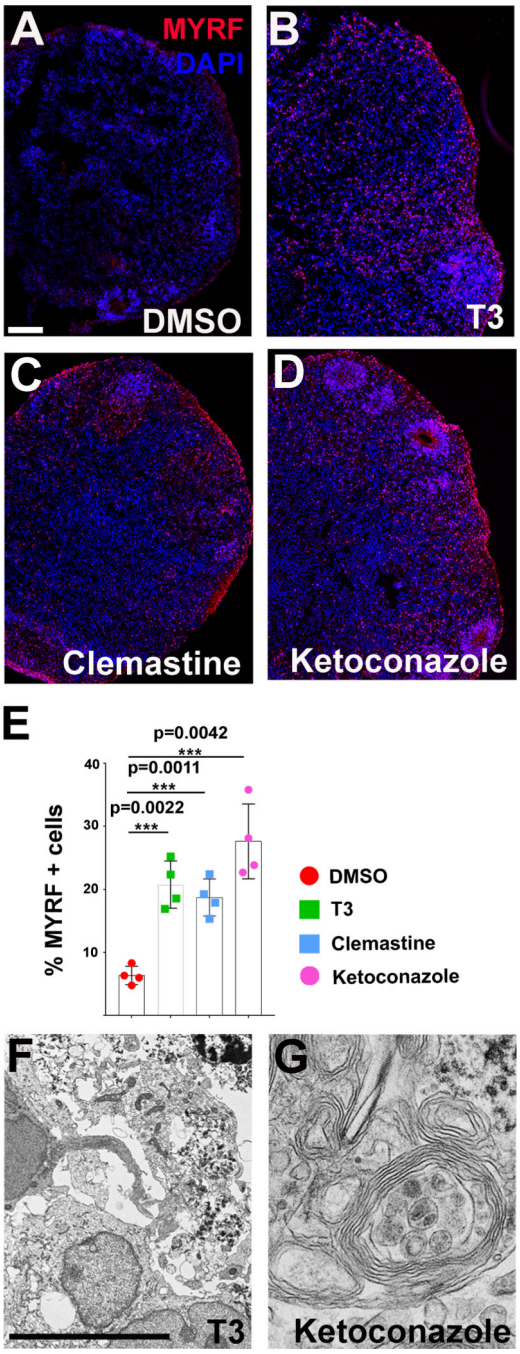

Figure 4 |. Promyelinating drugs promote the generation of oligodendrocytes in oligocortical spheroids.

a-d, Representative fluorescence images of week 14, H7 spheroids treated with PDGF/IGF-1 (from day 50–60) and either **a,** DMSO, **b,** T3, **c,** clemastine, or **d,** ketoconazole (from day 60–70). Whereas DMSO produced few MYRF-positive cells, T3, clemastine, and ketoconazole produced robust MYRF signal. Four spheroids from the same batch were used for analysis. Scale bar, 50um for **a-d**.

e, Quantification of MYRF from **a-d**. MYRF-positive cells were counted in four individual spheroids (n=4) per cell line (colored points) and averaged (white bars). Error bars are standard deviation and a two-tailed unpaired t-test with Welch's correction was performed. **f,** Representative EM of week 14, H7 spheroids generated with T3 (i.e. the standard oligocortical protocol) demonstrates an absence of myelin. Scale bar, 500nm for **f** and **g**. **g,** Representative EM of week 14, H7 spheroids generated with ketoconazole in lieu of T3 demonstrates robust production of non-compact myelin encircling multiple neuronal axons.

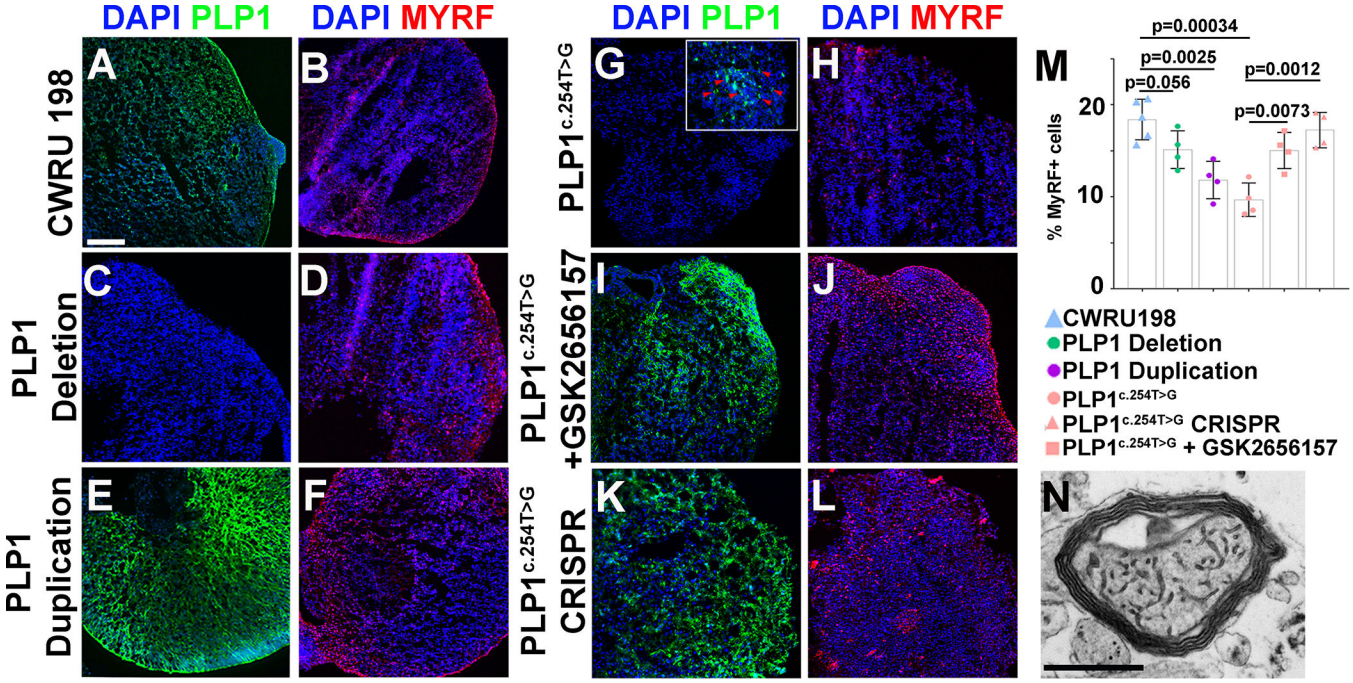

Figure 5 |. Oligocortical spheroids recapitulate a human myelin disease phenotype.

a-b, Representative fluorescence images of week 14, CWRU198 oligocortical spheroids immunostained for **a,** PLP1:green or **b,** MYRF:red demonstrates abundant oligodendrocytes and robust PLP1 expression. Scale bar, 50um for **a-l**. Five spheroids from the same batch were used for analysis.

c-d, Representative images of week 14, PLP1 deletion oligocortical spheroids immunostained for **c,** PLP1:green or **d,** MYRF:red demonstrates an expected lack of PLP1 despite abundant MYRF-positive oligodendrocytes. Four spheroids from the same batch were used for analysis.

e-f, Representative images of week 14, PLP1 duplication oligocortical spheroids immunostained for **e,** PLP1:green or **f,** MYRF:red demonstrates robust PLP1 expression despite a decrease in the abundance of MYRF-positive oligodendrocytes. Four spheroids from the same batch were used for analysis.

g-h, Representative images of week 14, PLP1 c.254T>G oligocortical spheroids immunostained for **g,** PLP1:green or **h,** MYRF:red demonstrates perinuclear retention of PLP1 and a decrease in MYRF-positive oligodendrocyte abundance. Four spheroids from the same batch were used for analysis.

i-j, Representative images of week 14, PLP1 c.254T>G oligocortical spheroids treated with GSK2656157 and immunostained for **i,** PLP1:green or **j,** MYRF:red demonstrates mobilization of PLP1 into oligodendrocyte process and rescue of MYRF-positive oligodendrocyte abundance. Four spheroids from the same batch were used for analysis.

k-l, Representative images of week 14, PLP1 CRISPR-corrected c.254TG>T oligocortical spheroids immunostained for **k,** PLP1:green or **l,** MYRF:red demonstrates rescue of both PLP1 perinuclear retention and oligodendrocyte abundance. Four spheroids from the same batch were used for analysis.

m, %MYRF-positive oligodendrocytes per organoid in **a-l**. MYRF-positive cells were counted from five individual spheroids of control line CWRU 198 (n=5) and four individual spheroids (n=4) per cell line (colored points) and averaged (white boxes). Error bars are standard deviation and a two tailed unpaired t-test with Welch's correction was performed. **n**, Representative EM of week 30, PLP1 CRISPR-corrected c.254G>T oligocortical spheroids demonstrates compact myelin encircling an axon. 3 spheroids from a single batch were used for EM analysis. Scale bar, 1um.